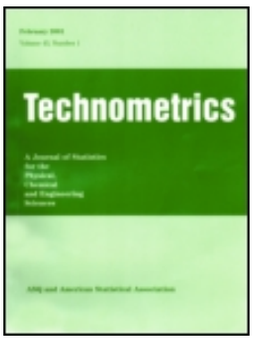

Technometrics

ISSN: 0040-1706 (Print) 1537-2723 (Online) Journal homepage: https://www.tandfonline.com/loi/utch20

Statistical Methods for Degradation Data With Dynamic Covariates Information and an Application to Outdoor Weathering Data

Yili Hong, Yuanyuan Duan, William Q. Meeker, Deborah L. Stanley & Xiaohong Gu

To cite this article: Yili Hong, Yuanyuan Duan, William Q. Meeker, Deborah L. Stanley & Xiaohong Gu (2015) Statistical Methods for Degradation Data With Dynamic Covariates Information and an Application to Outdoor Weathering Data, Technometrics, 57:2, 180-193, DOI: 10.1080/00401706.2014.915891

To link to this article: https://doi.org/10.1080/00401706.2014.915891

Supplementary materials for this article are available online. Please go to http://www.tandfonline.com/r/TECH

Statistical Methods for Degradation Data With Dynamic Covariates Information and an Application to Outdoor Weathering Data

Yili HONG and Yuanyuan DUAN

Department of Statistics
Virginia Tech
Blacksburg, VA 24061
(*yilihong@vt.edu*; *yyduan@vt.edu*)

William Q. MEEKER

Department of Statistics and Center
for Nondestructive Evaluation
Iowa State University
Ames, IA 50011
(*wqmeeker@iastate.edu*)

Deborah L. STANLEY and Xiaohong GU
Engineering Laboratory
National Institute of Standards and Technology
Gaithersburg, MD 20899
(*deborah.stanley@nist.gov*; *xiaohong.gu@nist.gov*)

Degradation data provide a useful resource for obtaining reliability information for some highly reliable products and systems. In addition to product/system degradation measurements, it is common nowadays to dynamically record product/system usage as well as other life-affecting environmental variables, such as load, amount of use, temperature, and humidity. We refer to these variables as dynamic covariate information. In this article, we introduce a class of models for analyzing degradation data with dynamic covariate information. We use a general path model with individual random effects to describe degradation paths and a vector time series model to describe the covariate process. Shape-restricted splines are used to estimate the effects of dynamic covariates on the degradation process. The unknown parameters in the degradation data model and the covariate process model are estimated by using maximum likelihood. We also describe algorithms for computing an estimate of the lifetime distribution induced by the proposed degradation path model. The proposed methods are illustrated with an application for predicting the life of an organic coating in a complicated dynamic environment (i.e., changing UV spectrum and intensity, temperature, and humidity). This article has supplementary material online.

KEY WORDS: Covariate process; Environmental conditions; Lifetime prediction; Organic coatings; System health monitoring; Usage history.

1. INTRODUCTION

1.1 Motivation

For products and systems with high reliability, it is challenging to do field reliability assessment in a timely manner based only on limited lifetime data. When available, degradation data provide a useful resource for obtaining reliability information because there are degradation measurements for each individual unit in the field before the individual unit fails. For products with degradation driven by usage and environmental conditions, information about these variables can be important for modeling the degradation process. For example, the degradation of organic coatings is primarily driven by ultraviolet (UV) exposure, while temperature and humidity are other important factors. There are many other more examples where degradation is driven by usage and environmental variables, such as the loss of light output from a light-emitting diode (LED) array, the decrease of power output of photovoltaic arrays, the corrosion in an oil transportation pipeline, the vibration from a bearing in a wind turbine, and the loss of color and gloss of an automobile coating.

Developments in technology allow many systems to collect and transmit massive amounts of information. It is common nowadays to dynamically record product/system usage and load as well as other environmental variables such as temperature and humidity, which we refer to as dynamic covariate information. For example, even a small device like a power inverter that is used in solar panel arrays can gather and transmit information on the output of power, the ambient temperature, and humidity every few seconds. The availability of such large-scale dynamic data creates many opportunities and challenges.

Dynamic covariate data contain rich information that can be useful for modeling and predicting product reliability. One can expect those units that are heavily used and are used under the most extreme environments to fail sooner than those units with lighter usage under normal environmental conditions. Thus, it is attractive to incorporate dynamic covariate information into

TECHNOMETRICS, MAY 2015, VOL. 57, NO. 2
DOI: 10.1080/00401706.2014.915891
Color versions of one or more of the figures in the article can be found online at *www.tandfonline.com/r/tech*.

degradation modeling and data analysis, especially when predictions are required for individual units.

Although not all systems will provide degradation data, there are many that will. Examples include power output from a satellite transmitter, power from solar cells, power from voltage inverters, light output from an LED array, number of paper jams per week in a printer/copier, rechargeable battery capacity, etc. The main goal of this article is to develop general models for analyzing degradation data and dynamic covariate information for a fleet of products. Based on the degradation data model, one can obtain estimates for the remaining lifetime distribution and predictions for the product population and for individual units in the field. We use data from an outdoor weathering experiment to illustrate the models and methods.

1.2 Related Literature

In the literature, general path models are commonly used to analyze degradation data (e.g., Lu and Meeker 1993). For a specified failure definition, the cumulative distribution function (cdf) of the lifetime distribution is induced by the parametric model for the degradation paths. Stochastic models are another class of models to analyze degradation data (e.g., Lawless and Crowder 2004). The stochastic model approach assumes that the data are generated from a stochastic process, such as a Wiener process, a gamma process, or an inverse Gaussian process. By the properties of the assumed underlying stochastic process, the cdf of the lifetime distribution can be obtained. Details on parameter estimation for various degradation models are available in chap. 13 of Bagdonavičius and Nikulin (2001a). Singpurwalla (1995) considered both univariate and multivariate survival models under dynamic environments. Zhou et al. (2014) applied functional data analysis approaches to degradation data modeling.

For degradation data analysis, covariate information and the modeling of covariates are available in several settings such as accelerated repeated-measure degradation tests (e.g., Meeker, Escobar, and Lu 1998; Bagdonavičius and Nikulin 2001b), accelerated destructive degradation tests (e.g., Escobar et al. 2003), and degradation-test experimental designs (e.g., Joseph and Yu 2006; Park and Padgett 2006). Bagdonavičius, Masiulaitytė, and Nikulin (2010) described a stochastic degradation model with time-varying covariates. The time-varying covariates are incorporated into the induced cdf of the degradation process through a cumulative damage model (see, e.g., Nelson 2001).

Little work has been done in degradation data modeling that also considers unit-to-unit or temporal variability for covariates. The modeling of the effect of the dynamics on degradation can provide valuable information in several areas. For example, degradation information is important in the area of system health monitoring or condition-based maintenance, where dynamic covariate information is available for continuously monitored systems. Thus, general models for analyzing degradation with dynamic covariate information need to be developed.

1.3 Overview

The rest of the article is organized as follows. Section 2 introduces a dataset collected from outdoor weathering of epoxy coating experiments conducted at the National Institute of Standards and Technology (NIST) as the motivating example. Section 2 also introduces the data structure and notation for degradation data with dynamic covariates. Sections 3 proposes a general additive model for incorporating dynamic covariate information into the degradation path model. Section 4 develops parameter estimation procedures. Section 5 uses simulation to validate the inference procedure. Section 6 describes parametric models for a multivariate covariate process and the corresponding procedures for parameter estimation. Section 7 develops procedures for failure-time distribution estimation based on the parametric models given in Sections 3 and 6. Section 8 contains some concluding remarks and describes possible areas for future research.

2. DATA

2.1 Outdoor Weathering Data

The illustrative application is based on an outdoor weathering dataset from a study conducted by scientists at NIST. The data were collected in a study of the service life of organic coatings in outdoor environments. Outdoor weathering experiments were carried out in Gaithersburg, MD, from 2002 through 2006. There were 36 specimens placed in outdoor environmental chambers on the roof of a building on the NIST campus, starting at different times over a period of approximately 5 years. The outdoor temperature, humidity, and ultraviolet (UV) spectrum and intensity were recorded over this period of time automatically by sensors. See Gu et al. (2009) for more details. In this application, all units were exposed at the same location. There could be various exposure patterns in different applications, as discussed in Section 7.1.

The degradation measurement was done periodically (at intervals of several days) for each specimen using Fourier transform infrared (FTIR) spectroscopy. Special compounds or structures cause peaks on the FTIR spectrum. The height of a peak is proportional to the concentration of a certain compound or structure. Degradation will cause decrease in the concentration. Thus, the changes in the height of the peak at a particular point of the FTIR spectrum can be used as a degradation measurement. For illustration, we consider the degradation that occurs at damage number 1250 cm^{-1} on the FTIR spectrum, which is attributed to C–O stretching of aryl ether. Figure 1(a) shows nine representative degradation paths from nine specimens, started at different times of the year and in different years. A large part of the variability in these data is due to the varying amount of UV exposure during the nine different periods of time. The time scale of the degradation measurement, denoted by t, is the time in days since the start of exposure for a specimen.

The samples used for experiments were specially fabricated using a model epoxy that was known to degrade rapidly. Also, the samples were very thin. In this manner, similar to an accelerated test, experimental information would be obtained on individual units in a timely manner (i.e., in months instead of in years). Although the specimens are different from coatings used in real applications, the degradation mechanism is the same.

For the dynamic covariate information, Figure 1(b)–1(d) shows the daily values of the UV dosage, temperature (in degrees Celsius °C), and relative humidity (RH) (in

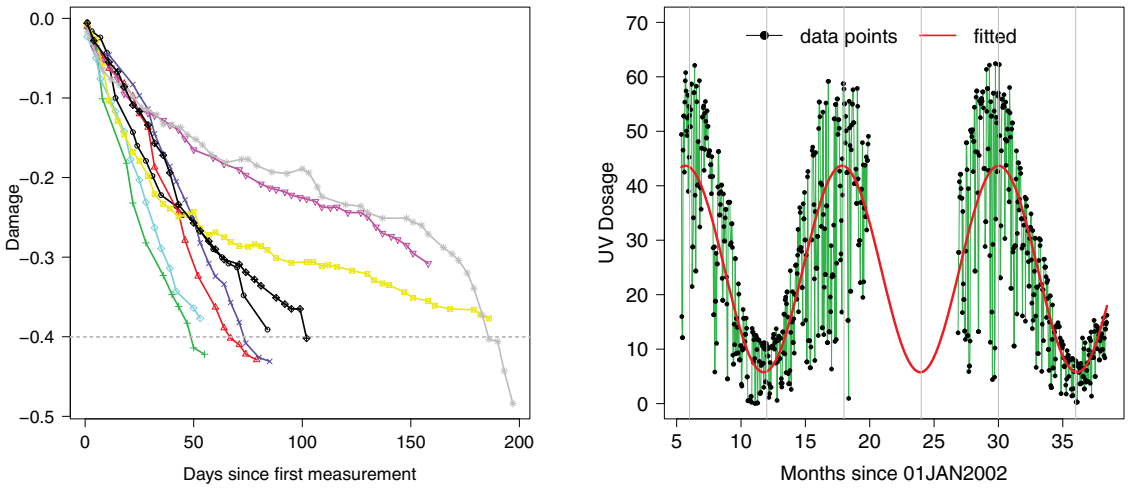

(a) Degradation measurements (b) Daily UV dosage

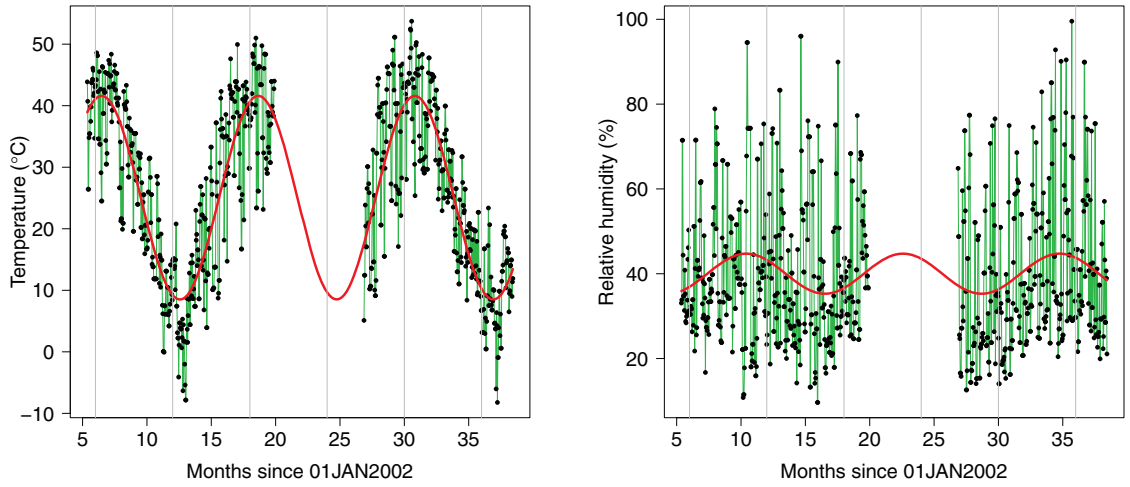

(c) Daily temperature (d) Daily RH

Figure 1. Plot of nine representative degradation paths and dynamic covariate information. The black dots/lines show the daily values, connected by line segments. The vertical lines show 6 months, 12 months, . . ., from January 1, 2002. The thick smooth curves show the fitted mean structures.

percentage %), respectively. The time scale for those covariates, denoted by τ, is the time in days since January 1, 2002. Although the covariates were recorded at much finer resolutions, we aggregated them into daily values for convenience of modeling. Scientifically, an appropriate summary of UV exposure is the UV dosage that is proportional to the number of photons absorbed into the degrading material (such photons cause the damage). The daily UV dosage at day τ is computed by $\int_{\tau}^{\tau+1}\int_{\lambda_{\min}}^{\lambda_{\max}} E(\zeta,\lambda)\left[1-e^{A(\lambda)}\right]d\lambda d\zeta$, where the spectral irradiance $E(\zeta,\lambda)$ is the dose (proportional to the number of photons hitting the surface) at time ζ from sun light with wavelength λ, $[1-e^{A(\lambda)}]$ is the absorbance rate for different wavelengths, and $\lambda_{\min}=300$ nm and $\lambda_{\max}=532$ nm give the wavelength limits. Wavelengths above 532 nm are not harmful and wavelengths below 300 nm are generally filtered by atmospheric ozone. The UV spectrum and intensity values were recorded at 12 min intervals but were aggregated into daily dosage values. For the period between day 598 and day 805, the covariate information is not available because there was no experimental data being collected during that period.

As it can be seen in Figure 1, the environmental covariates show seasonal patterns and also different degrees of variability during different time periods. For example, the UV dosage shows more variability during summer time than during winter time. Due to different starting times, each specimen has its own profile of dynamic covariate information, resulting in different rates of degradation, as can be seen from Figure 1(a). For example, those units started in summers initially degraded much more rapidly than those started in winters.

2.2 Notation for the Data

Here, we introduce some notation for the degradation data model and the dynamic covariate model. Let $X(t)=[X_1(t),\ldots,X_p(t)]'$ be the usage/environmental information at time t, where p is the number of covariates. Let $\boldsymbol{X}(t)=$

$\{X(s) : 0 \le s \le t\}$ be the history of the covariate process, which records the dynamic information from time 0 to time t.

Suppose there are n units/specimens in the field. For unit i, denote the degradation measurements at time t_{ij} by $y_i(t_{ij})$, $i = 1, \ldots, n$, $j = 1, \ldots, n_i$, and n_i is the number of time points where degradation measurements were taken. The value of covariate l for unit i at the time s is denoted by $x_{il}(s)$. The history of the covariate process for unit i is denoted by $\boldsymbol{x}_i(t_{in_i}) = \{x_i(s) : 0 \le s \le t_{in_i}\}$, which records the dynamic information from time 0 to time t_{in_i} for unit i. Here $x_i(s) = [x_{i1}(s), \ldots, x_{ip}(s)]'$.

3. MODEL FOR A DEGRADATION PATH

3.1 General Path Model

Let $\mathcal{D}(t); t > 0$ be the actual degradation path and let

$$y(t) = \mathcal{D}(t) + \epsilon(t) \tag{1}$$

be the degradation measurement at time t. The degradation model implies a degradation path $\mathcal{D}(t)$ for each unit in the population. We assume throughout that the degradation path is decreasing and the modifications are straightforward for an increasing degradation path. When the degradation level $\mathcal{D}(t)$ first falls below the failure-definition level $\mathcal{D}_f$, a soft failure occurs and we say that the unit has failed. The first crossing time is denoted by $t_{\mathcal{D}}$ and

$$t_{\mathcal{D}} = \min\{t : \mathcal{D}(t) \le \mathcal{D}_f\}.$$

The failure-time random variable T is defined as the collection of the failure times $t_{\mathcal{D}}$ for all of the units in the population. The cdf of T is $F(t) = \Pr(T \le t)$. The estimate of $F(t)$ is used for the reliability prediction for the population, which is obtained by using both the degradation measurements and the dynamic covariate information.

3.2 Modeling Degradation Path With Dynamic Covariates

Here, we introduce a general additive model to incorporate dynamic covariate information into the degradation path model. In particular, the observed degradation path, conditional on the dynamic covariate information, is modeled as

$$y_i(t_{ij}) = D[t_{ij}; \boldsymbol{x}_i(t_{ij})] + R(t_{ij}; w_i) + \varepsilon_i(t_{ij}). \tag{2}$$

The corresponding model for the actual degradation path is $D[t_{ij}; \boldsymbol{x}_i(t_{ij})] + R(t_{ij}; w_i)$. The first component $D[t_{ij}; \boldsymbol{x}_i(t_{ij})] = \beta_0 + \sum_{l=1}^{p} \int_0^{t_{ij}} f_l[x_{il}(\tau); \beta_l] d\tau$ incorporates the dynamic covariates into the degradation path through a covariate-effect function $f(\cdot)$. Here, β_0 is the initial level of degradation, and β_l denotes the parameter(s) in covariate-effect function $f_l(\cdot)$, $l = 1, \ldots, p$. The coefficient vector for the initial degradation and covariate effects is denoted by $\boldsymbol{\beta} = (\beta_0, \beta_1', \ldots, \beta_p')'$. For covariate l, the function $f_l[x_{il}(\tau); \beta_l]$ represents the effect of $x_{il}(\tau)$ at time τ on the degradation process. Thus, $\int_0^t f_l[x_l(\tau); \beta_l] d\tau$ is the cumulative effect of x_l on the degradation process up to time t.

The cumulative damage model is motivated by the cumulative damage model for the accelerated failure-time model in (Nelson 2001, chap. 10). For certain degradation mechanisms (e.g., wear out, crack growth, and the decomposition of chemical structures), the assumption of cumulative effects is appropriate. In the motivating application of this article, the environmental variables cause the loss of certain chemical structures in the coating, which reduces the concentration of certain chemical compounds over the time. Thus, the assumption of the cumulative effects is appropriate for the application.

The second component $R(t; w_i)$ is used to capture random departures from the mean structure $D[t; \boldsymbol{x}_i(t)]$. In particular, an individual random effect w_i is used to account for unit-to-unit variability caused by unobservable factors. A simple but useful form of $R(t_{ij}; w_i)$ is $R(t_{ij}; w_i) = w_{0i} + w_{1i} t_{ij}$, where $w_i = (w_{0i}, w_{1i})'$, which has nice interpretation. In particular, w_{0i} and w_{1i} can be interpreted as individual random effects for the initial degradation and the time trend, respectively. A linear additive term also makes parameter estimation convenient. The random effect w_i is modeled by a bivariate normal distribution $\mathrm{N}(0, \Sigma_w)$. Let $\boldsymbol{\sigma}_w$ be a general notation for the unique parameters in Σ_w. The third component $\varepsilon_i(t_{ij})$ in (2) is the noise term. In literature, for example, Meeker and Escobar 1998, the $\varepsilon_i(t_{ij})$'s are often modeled to be independent and identically distributed as $\mathrm{N}(0, \sigma_\varepsilon^2)$.

3.3 Functional Forms for Covariate-Effect Function $f(\cdot)$

Two approaches are available for choosing the functional form for the covariate-effect function $f(\cdot)$. The first approach is based on models motivated by physical, chemical, and engineering knowledge. For example, if there is dynamic information on temperature, the Arrhenius relationship (e.g., Meeker and Escobar 1998, p. 472) can sometimes be used to model the effect of temperature on the rate of a degradation process.

When there is not sufficient knowledge about the form of $f(\cdot)$ from physical/engineering knowledge or when such models do not fit the data well, nonparametric methods can be used. For this approach, the function $f(\cdot)$ can be estimated as a linear combination of spline bases. Because most physical variables have a particular relationship with the degradation process (e.g., the degradation rate is increasing as the temperature is increasing), we apply shape restrictions on $f(\cdot)$. To obtain functional forms for $f(\cdot)$ with different shape restrictions (e.g., monotonic increasing, decreasing, or convex), we use shaped-restricted splines described in Meyer (2008), which are flexible enough to model constrained functions. In particular, a monotone function is estimated by a linear combination of the basis functions (I-splines) and a constant function. To constrain the estimate to be monotone increasing, the coefficients of the basis functions must be nonnegative (the coefficient of the constant function is not constrained). A convex regression function is estimated using linear combinations of the basis functions (C-splines) with nonnegative coefficients, plus an unrestricted linear combination of the constant function and the identity function $g(x) = x$. Details for spline basis computation are given in supplementary Section 1.

For the outdoor weathering data, the degradation path of the FTIR damage number 1250 cm^{-1} is monotone decreasing. Higher UV dosage or temperature tends to cause larger damage rates. Thus, the effects of UV dosage and temperature are

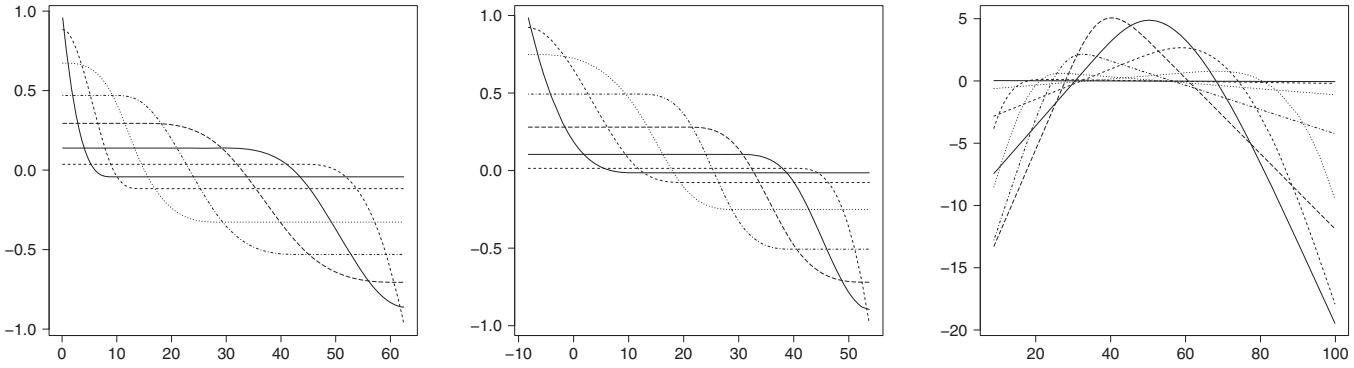

Figure 2. Splines bases for the covariate effects of UV dosage, temperature, and RH.

constrained to be monotone decreasing in UV dosage and temperature. The effect of RH is constrained to be concave, based on a graphical analysis of the indoor weathering data in Gu et al. (2009) where the RH was controlled (along with other experimental variables) at different levels for several groups of test units. Figure 2 shows the spline bases for the covariate effects of UV dosage, temperature, and RH. Note that the spline bases in Figure 2(a) and 2(b) are different because their computations are based on different covariates (i.e., UV dosage and temperature).

4. DEGRADATION PATH MODEL PARAMETER ESTIMATION

4.1 Parameter Estimation

Because the degradation data and dynamic covariate processes are observed at discrete points in time, the discrete-data version of model (2) is obtained by replacing $D[t_{ij}; \boldsymbol{x}_i(t_{ij})]$ with $D[t_{ij}; \boldsymbol{x}_i(t_{ij})] = \beta_0 + \sum_{l=1}^{p} \sum_{\tau_{ik} \le t_{ij}} f_l[x_{il}(\tau_{ik}); \beta_l](\tau_{ik} - \tau_{i,k-1})$. Here, τ_{ik} are the time points where the covariate process was recorded for unit k, with convention that $\tau_{i0} = 0$. Let $\boldsymbol{\theta}_D = \{\boldsymbol{\beta}, \boldsymbol{\sigma}_w, \sigma_\varepsilon\}$ be the collection of unknown parameters. The maximum likelihood (ML) method is used for parameter estimation. Given the observed covariate process history, the likelihood is

$$\begin{aligned} &L(\boldsymbol{\theta}_D | \text{covariate history}) \\ &= \prod_{i=1}^{n} \int_{w_i} \left[\prod_{t_{ij} \le t_{in_i}} \frac{1}{\sigma_\varepsilon} \phi \left\{ \frac{B[y_i(t_{ij}); \boldsymbol{x}_i(t_{ij}), w_i]}{\sigma_\varepsilon} \right\} \right. \\ &\quad \left. \times g_{w_i}(w_i; \boldsymbol{\sigma}_w) \right] dw_i, \end{aligned} \tag{3}$$

where $B[y_i(t_{ij}); \boldsymbol{x}_i(t_{ij}), w_i] = y_i(t_{ij}) - D[t_{ij}; \boldsymbol{x}_i(t_{ij})] - R(t_{ij}; w_i)$, $\phi(\cdot)$ is the probability density function (pdf) of a N(0, 1) distribution, and $g_{w_i}(\cdot)$ is the pdf of a N(0, Σ_w) distribution. The ML estimate $\widehat{\boldsymbol{\theta}}_D$ is obtained by finding the value of $\boldsymbol{\theta}_D$ that maximizes (3). Note that we are conditioning on the entire covariate history when we model the degradation process.

The maximization of (3), in general, is nontrivial because numerical methods such as quadrature (e.g., Liu and Pierce 1994) are needed to evaluate the integral in the likelihood function. When the random component is modeled as a linear function of w_i, the model in (2) becomes a linear mixed-effect model with constraints on the parameters. Davidov and Rosen (2011) proposed to use constrained quadratic programming to find the ML estimates of the unknown parameters with constraints in linear mixed-effect models. For better computational efficiency, we propose to replace the constrained quadratic programming by the mixed primal-dual bases algorithm in Fraser and Massam (1989).

In particular, with shape-restricted splines (i.e., $f_l[x_{il}(\tau_{ik}); \beta_l] = \sum_{q=1}^{Q_l} B_{lq}[x_{il}(\tau_{ik})]\beta_{lq}$) and the random component $R(t_{ij}; w_i) = w_{0i} + w_{1i} t_{ij}$, the model in (2) can be represented by

$$y_i(t_{ij}) = \beta_0 + \sum_{l=1}^{p} \sum_{q=1}^{Q_l} G_{lq}(t_{ij})\beta_{lq} + w_{0i} + w_{1i} t_{ij} + \varepsilon_i(t_{ij}). \tag{4}$$

Here, $B_{lq}[x_{il}(\tau_{ik})]$ is the value of the corresponding spline basis evaluated at $x_{il}(\tau_{ik})$, β_{lq}'s are spline coefficients, $G_{lq}(t_{ij}) = \sum_{\tau_{ik} \le t_{ij}} B_{lq}[x_{il}(\tau_{ik})](\tau_{ik} - \tau_{i,k-1})$, and Q_l is the number of spline bases for covariate l. Let $\boldsymbol{y}_i = (y_{i1}, \ldots, y_{in_i})'$,

$$\boldsymbol{X}_i = \begin{bmatrix} 1 & G_{11}(t_{i1}) & \cdots & G_{1Q_1}(t_{i1}) & \cdots & G_{p1}(t_{i1}) & \cdots & G_{pQ_p}(t_{i1}) \\ \vdots & \vdots & \ddots & \vdots & \ddots & \vdots & \ddots & \vdots \\ 1 & G_{11}(t_{in_i}) & \cdots & G_{1Q_1}(t_{in_i}) & \cdots & G_{p1}(t_{in_i}) & \cdots & G_{pQ_p}(t_{in_i}) \end{bmatrix},$$

$$\boldsymbol{Z}_i = \begin{bmatrix} 1 & t_{i1} \\ \vdots & \vdots \\ 1 & t_{in_i} \end{bmatrix},$$

and $\boldsymbol{\varepsilon}_i = [\varepsilon_i(t_{i1}), \ldots, \varepsilon_i(t_{in_i})]'$. Using this notation, the model in (4) can be expressed as $\boldsymbol{y}_i = \boldsymbol{X}_i\boldsymbol{\beta} + \boldsymbol{Z}_i w_i + \boldsymbol{\varepsilon}_i$. Note that the variance-covariance matrix of $\boldsymbol{y}_i$ is $\Sigma_i = \boldsymbol{Z}_i \Sigma_w \boldsymbol{Z}_i' + \sigma_\epsilon^2 \boldsymbol{I}_{n_i}$, where

$$\Sigma_w = \begin{bmatrix} \sigma_0^2 & \rho\sigma_0\sigma_1 \\ \rho\sigma_0\sigma_1 & \sigma_1^2 \end{bmatrix}$$

and $\boldsymbol{I}_{n_i}$ is an $n_i \times n_i$ matrix. Let $\boldsymbol{\sigma}_w = (\sigma_0, \sigma_1, \rho)'$. Some components of $\boldsymbol{\beta}$ are constrained to be nonnegative to produce a shape-restricted covariate-effect function. Without loss of generality, let $\boldsymbol{\beta} = (\boldsymbol{\beta}_u', \boldsymbol{\beta}_c')'$, where $\boldsymbol{\beta}_u$ and $\boldsymbol{\beta}_c$ represent unconstrained and constrained parameters, respectively. The estimation algorithm is as follows.

Algorithm 1:

1. Obtain initial values of $\boldsymbol{\sigma}_w$ and σ_ε, which can be done by fitting the unconstrained linear mixed-effect model.
2. Compute $\Sigma_i = \boldsymbol{Z}_i \Sigma_w \boldsymbol{Z}_i' + \sigma_\epsilon^2 \boldsymbol{I}_i$.
3. With Σ_i computed in Step 2, use the mixed primal-dual bases algorithm to obtain the estimate of $\boldsymbol{\beta}$ by minimizing $\sum_{i=1}^{n} (\boldsymbol{y}_i - \boldsymbol{X}_i\boldsymbol{\beta})' \Sigma_i^{-1} (\boldsymbol{y}_i - \boldsymbol{X}_i\boldsymbol{\beta})$ subject to the constraints that the elements of $\boldsymbol{\beta}_c$ are greater than or equal to 0.
4. Fit a linear mixed-effect model $\widehat{\boldsymbol{\varepsilon}}_i = \boldsymbol{Z}_i w_i + \boldsymbol{\varepsilon}_i$ with $\widehat{\boldsymbol{\varepsilon}}_i = \boldsymbol{y}_i - \boldsymbol{X}_i \widehat{\boldsymbol{\beta}}$ to obtain updated estimates of $\boldsymbol{\sigma}_w$ and σ_ε.
5. Repeat Steps 2 to 4 until convergence.

Making inferences based on the constrained ML estimator is not straightforward. Some elements of the ML estimate vector may be on the boundary of the parameter space. Although asymptotic theory is available for constrained ML estimators (e.g., Self and Liang 1987), the bootstrap method provides a flexible and easy-to-implement alternative. The bootstrap inference procedure is also somewhat robust to model departures. After being adjusted by a method that is similar to Carpenter, Goldstein, and Rasbash (2003), the residuals and estimated random effects are sampled with replacement to construct a bootstrap sample. As pointed out by Morris (2002), direct resampling (i.e., without appropriate adjustment) of residuals and estimated random effects will result in confidence intervals (CIs) that are too narrow. The estimation procedure in Algorithm 1 is then applied to the bootstrapped data to obtain bootstrapped values of parameter estimates. The resampling process is repeated a large number of the times and bias-corrected CIs are constructed based on the bootstrapped parameter estimates (Efron and Tibshirani 1993). The details of the bootstrap algorithm and CI procedure are described in Algorithms 3 and 4 in supplementary Section 2. The performance of Algorithm 1 and the bootstrap CI procedure will be investigated through simulations in Section 5.

4.2 Estimation for Weathering Data

For the outdoor weathering application, the spline bases shown in Figure 2 were used to estimate the effect of UV dosage, temperature, and RH. The parameter estimates are obtained by using Algorithm 1. The estimates and CIs for β_0, σ_0, σ_1, ρ, and σ_ε are shown in Table 1. The CIs were obtained from 10,000 bootstrap repeats. The bootstrap took about 4 h using R parallel computing with 20 cores with Intel CPU (Xeon, E6540, 2.00GHz). Figure 3 shows the estimated effect functions for UV dosage, temperature and RH, and the corresponding approximate 95% pointwise CIs. Figure 3(a) shows that larger UV dosages lead to more damage. The UV dosage has a large effect on the damage rate, relative to temperature and RH. Figure 4 shows the plot of degradation measurements and fitted degradation path for the nine representative specimens shown in Figure 1. The figure shows that the general path model fits the degradation data well. We also checked the Q–Q plot of the residuals (see supplementary Figure 5) and the plot indicates that the normal distribution assumption holds well.

For the selection of spline orders/degrees, a spline order/degree of two or three is generally sufficient to ensure enough smoothness. We used the Akaike information criterion (AIC; e.g., Eilers and Marx 1996) to select the spline orders and knots. We chose the knot locations based on equal sample quantiles, which places the knots in places where there is a sufficient amount of covariate information. For example, for four knots ($b = 4$), the locations were chosen as the 0.2, 0.4, 0.6, and 0.8 sample quantiles of the covariate values. For splines with different orders, we plotted the AIC values as a function of the number of spline knots (see supplementary Figure 6). Based on the results, we choose order three splines with four knots (i.e., $h = 3$ and $b = 4$) for the weathering data. An alternative approach is to use the asymptotically optimal number for b, in which $b \approx c^{1/(2h+1)}$ (e.g., Meyer 2008). Here, the sample size c is taken to be the number of time points where the covariates are recorded. For the weathering data, there are 676 time points. With $h = 3$, the number of knots is $b = 3$ for the covariates in the weathering data, which is very close to the selection by the AIC criterion.

We also did a sensitivity analysis on spline orders and the number of interior knots (see supplementary Figure 7). The figure shows that the estimated covariate-effect functions are insensitive to different choices of spline orders and the number of knots. This observation is consistent with the comments in Meyer (2008), which points out that the estimated functions are relatively insensitive to the number of knots, largely due to the shape restrictions.

Table 1. Parameter estimates and approximate 95% CIs for β_0, σ_0, σ_1, ρ, and σ_ε

			95% Bootstrap CI	
Parameter	Estimate	Standard error	Lower	Upper
β_0	–0.04164	0.00386	–0.04946	–0.03429
σ_0	0.02160	0.00318	0.01540	0.02775
σ_1	0.00067	0.00010	0.00049	0.00087
ρ	–0.47793	0.15143	–0.68934	–0.06847
σ_ε	0.01769	0.00048	0.01688	0.01880

5. SIMULATION STUDY

The estimation procedure in Section 4.1 involves random effects and point estimates that may be on a constraint boundary. Thus, we conduct a simulation to study the performance of the estimation procedure. Specifically, we investigate the mean square error (MSE) of point estimators and coverage probability (CP) of the bias-corrected bootstrap CI procedure.

5.1 Simulation Model and Setup

Although Algorithm 1 is reasonably fast, the evaluation of the CP of the bootstrap CI procedure is computationally demanding. To ease the computational burden, we consider a single covariate (UV), order two splines with two interior knots, and a simplified random component to simplify computations. All units are exposed to the same UV profile for 200 days. We use the first 200 day UV information from the weathering data as the UV exposure profile for the units in the simulation. The true model used in the simulation is

$$y_i(t_{ij}) = \beta_0 + \int_0^{t_{ij}} f[x_i(\tau); \beta] d\tau + w_{1i} t_{ij} + \varepsilon_i(t_{ij}), \quad (5)$$

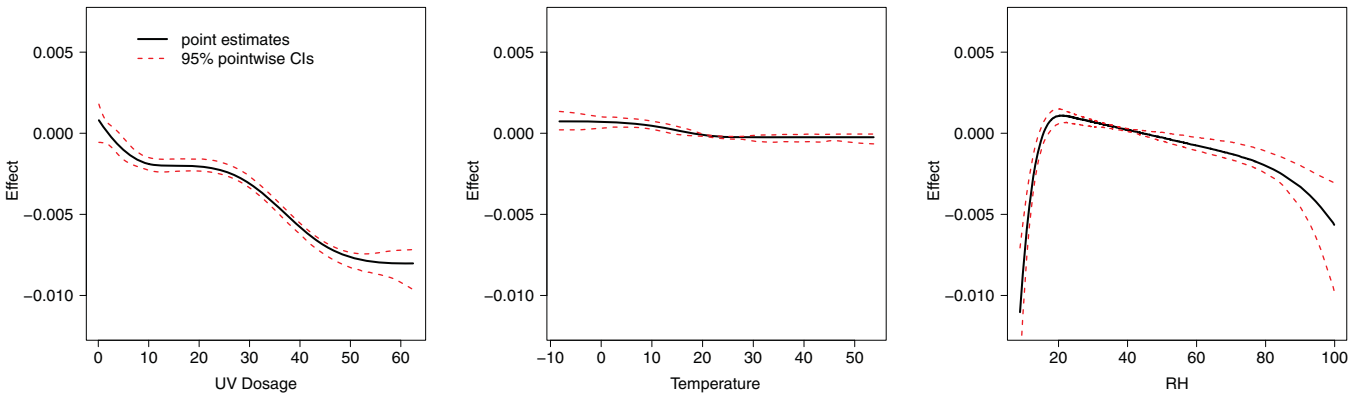

Figure 3. Estimated covariate-effect functions for UV dosage, temperature, and RH, and the corresponding approximate 95% pointwise CIs.

where $f[x_i(\tau_{ik}); \beta] = \sum_{q=1}^{5} B_q[x_i(\tau_{ik})]\beta_q$ is the UV effect function, $B_q[x_i(\tau_{ik})]$'s are the spline bases, $w_{1i} \sim \mathrm{N}(0, \sigma_1^2)$, and $\varepsilon_i(t_{ij}) \sim \mathrm{N}(0, \sigma_\varepsilon^2)$. Note that the $y_i(t_{ij})$'s from the same unit i in model (5) are correlated due to the random slope w_{1i}. The true values of the parameters are set to $\beta_0 = -0.03$, $\beta = (0.005, 0.003, 0, 0.006, 0)'$, $\sigma_1 = 0.001$, and $\sigma_\varepsilon = 0.02$ to mimic the setting of the weathering data. Figure 5 shows the spline bases (the constant basis is not shown) and the UV effect function used in simulation. The UV effect function is obtained as a linear combination of spline bases with coefficient β. Because the main purpose of the simulation is to verify the inference for the nonstandard situation, we set two elements of β to be zero, which are on the boundary of the constrained parameter space.

We considered six scenarios. The numbers of experimental units are chosen to be $n = 20$, 50, and 100. For each sample size, the numbers of degradation measurement points are chosen to be $m = 25$ and 50. In practice, m is related to how

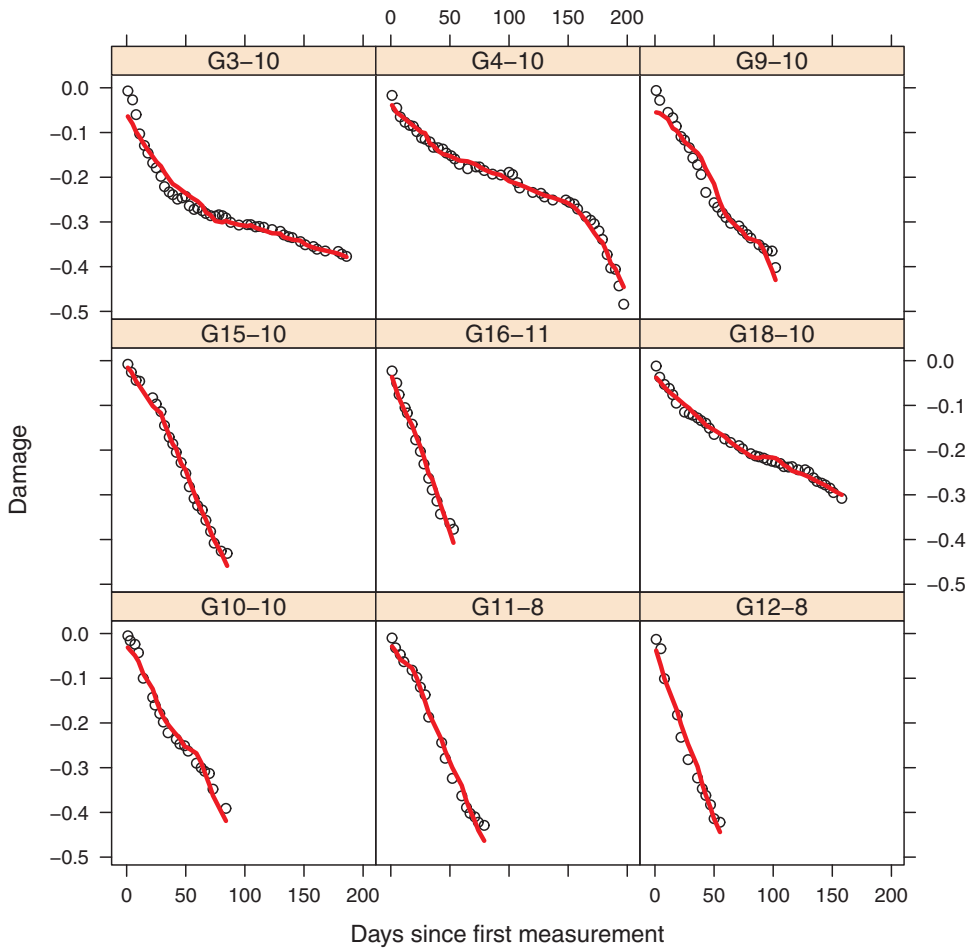

Figure 4. Plot of degradation measurements and fitted degradation path for the nine representative specimens shown in Figure 1.

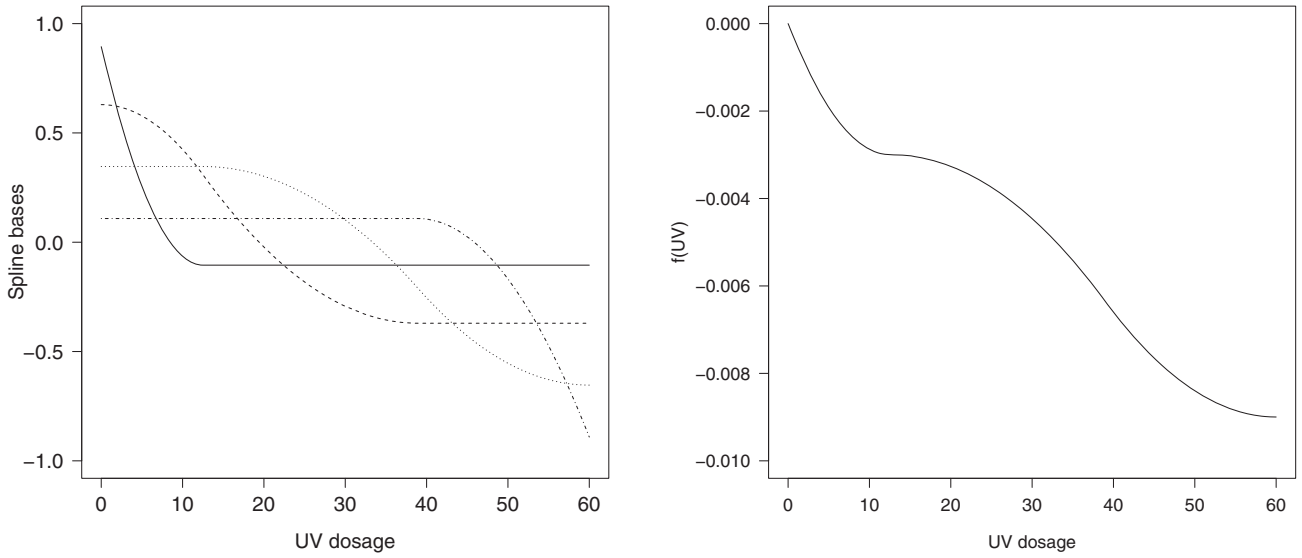

(a) Spline bases (b) UV effect function

Figure 5. Spline bases (left) and the UV effect function (right) used in simulation.

frequently measurements are taken. For each scenario, a dataset is simulated and Algorithms 1 and 4 (Algorithm 4 is in supplementary Section 2) are used to obtain the point estimates and CIs, respectively. A repeat of 600 datasets is used to obtain the estimates of the relative root MSE (RMSE) of point estimators and CP of CI procedures. The relative RMSE is defined as the square root of the MSE divided by the absolute value of the true parameter value. The CIs were obtained from 2000 bootstrap repeats.

5.2 Simulation Results

Figure 6 shows the estimated relative RMSE of the parameter estimators and the CP of CI procedure based on 600 repeats for β_0, σ_1, and σ_ε. Figure 7 shows the estimated relative RMSE for the UV effect function estimator and CP for the pointwise CI procedure for the UV effect function based on 600 repeats for the six scenarios. Based on the simulation results, we find that the relative RMSE of the point estimators of the parameters and the UV effect function generally decrease as n and m increase. The CP of the CI procedures converge to the nominal 95% level as n and m increase. The CP of the CI procedure for σ_1 is poor when $n = 20$ but it improves when n increases. The CP of the pointwise CI procedure for the UV effect function is around 90% when $n = 20$ and it is around 95% when $n = 100$. Overall, the simulation study shows that the performance of estimation and bootstrap CI procedure are good. Supplementary Section 3 gives all the details about the simulation results including bias, variance, and MSE for each of the parameters.

6. MODEL FOR MULTIVARIATE COVARIATE PROCESS

6.1 General Strategy for Covariates Modeling

To predict a degradation path into the future, it is necessary to have a parametric model that can adequately predict the covariate process. In general, the following parametric structure for $X(t)$ can be used for each individual unit, $X(t) = m(t; \boldsymbol{\eta}) + a(t)$, where $m(t; \boldsymbol{\eta})$ is the mean function with parameter $\boldsymbol{\eta}$ and some components of $\boldsymbol{\eta}$ can be random to allow for population unit-to-unit (or time period-to-time period in our application) variability for the covariate process. Depending on the application, the parametric form for $m(t; \boldsymbol{\eta})$ can be specified. For example, the environmental temperature of an individual unit can be modeled as $X(t) = \text{Trend}(t) + \text{Seasonal}(t) + a(t)$, where Trend$(t)$ is the long-term trend and Seasonal(t) is a periodic seasonal term. The error term $a(t)$ is assumed to be a stationary process. In some applications, $a(t)$ for different values of t can be modeled as

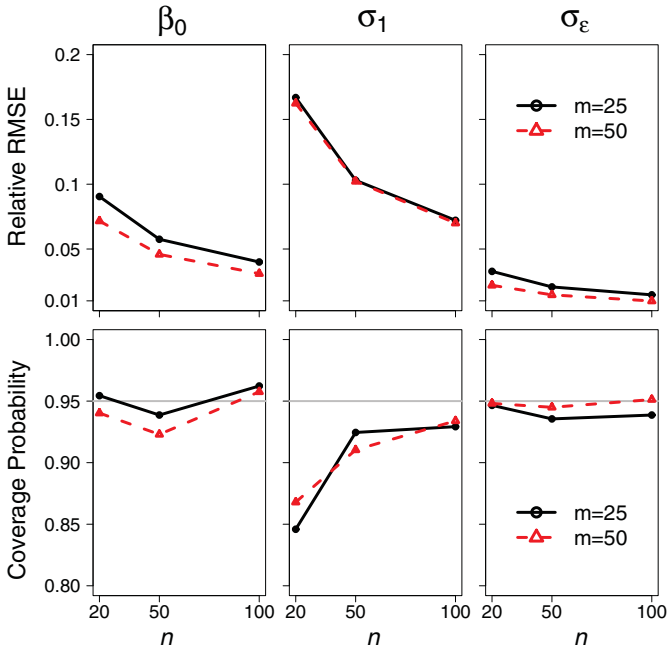

Figure 6. Estimated relative RMSE of the parameter estimators and CP of CI procedure.

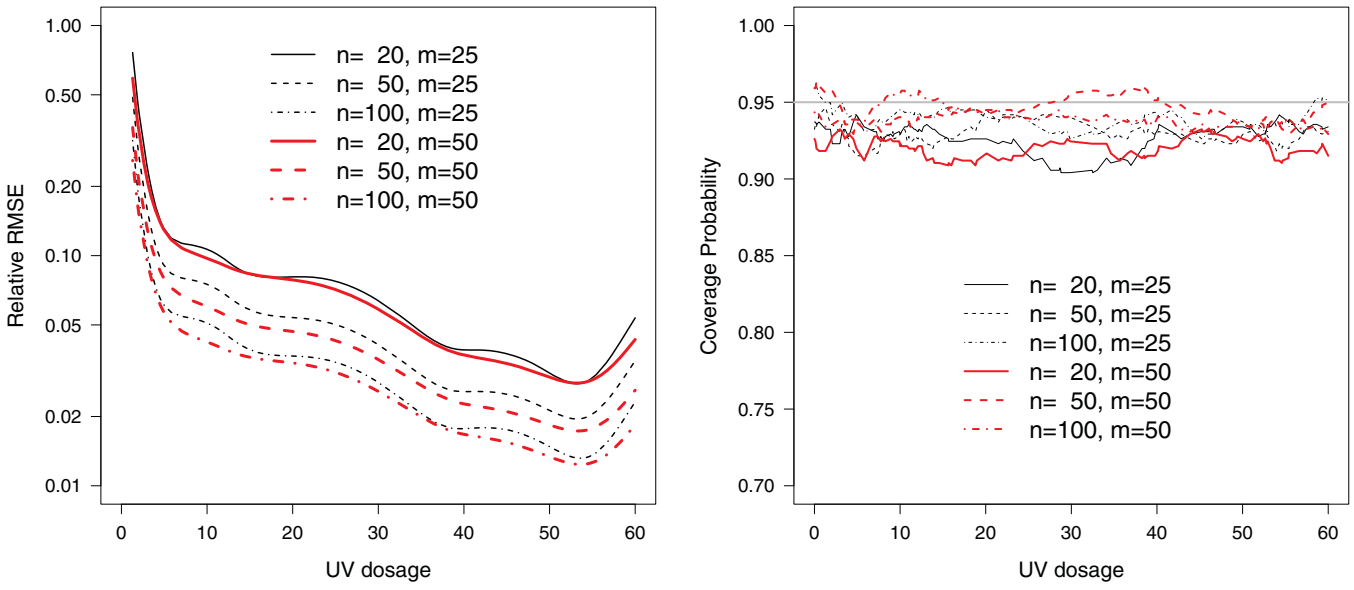

(a) Relative RMSE (b) CP

Figure 7. Estimated relative RMSE for estimator (left) and CP for pointwise CI for UV effect function (right).

independently and identically distributed with $N(0, \Sigma_a)$, where Σ_a is the covariance matrix. The vector autoregressive (VAR) time series models in Reinsel (2003) can be used if more complicated structures are needed for modeling $a(t)$.

6.2 Parametric Models for Covariates for Outdoor Weathering Data

For each application, a special modeling effort will be needed to capture the unique features in the covariate process. Here, we present the modeling of the environmental variables in the outdoor weathering data. Let $x_1(\tau)$, $x_2(\tau)$, and $x_3(\tau)$ be the values of UV dosage, temperature, and RH at time τ, respectively. For these three variables, there is no significant time trend but the seasonal effect is evident. For time series with a seasonal component, combinations of sine and cosine functions are commonly used to capture the seasonal component (e.g., Campbell and Diebold 2005).

Based on an initial analysis of the covariates in the weathering data, a single sine function is adequate to describe the mean structure of $x_1(\tau)$, $x_2(\tau)$, and $x_3(\tau)$. There is also a seasonal pattern in the process variance. For example, there is more variability in UV dosage during the summer months than during the winter months. Thus, a seasonal component is also added to the variance structure. In particular, the multivariate time series is modeled by

$$\begin{bmatrix} x_1(\tau) \\ x_2(\tau) \\ x_3(\tau) \end{bmatrix} = \begin{bmatrix} \mu_1 + \kappa_1 \sin\left[\frac{2\pi}{365}(\tau - \eta_1)\right] \\ \mu_2 + \kappa_2 \sin\left[\frac{2\pi}{365}(\tau - \eta_2)\right] \\ \mu_3 + \kappa_3 \sin\left[\frac{2\pi}{365}(\tau - \eta_3)\right] \end{bmatrix}$$

$$+ \begin{bmatrix} \left(1 + \nu_1\left\{1 + \sin\left[\frac{2\pi}{365}(\tau - \varsigma_1)\right]\right\}\right)\varepsilon_1(\tau) \\ \left(1 + \nu_2\left\{1 + \sin\left[\frac{2\pi}{365}(\tau - \varsigma_2)\right]\right\}\right)\varepsilon_2(\tau) \\ \varepsilon_3(\tau) \end{bmatrix}. \quad (6)$$

The $\sin(\cdot)$ function with a period of 365 days is used to capture the seasonal pattern in the covariates. For the UV dosage and temperature, extra terms are used to capture the nonhomogeneity of variance over time. A likelihood ratio test suggested that the seasonal pattern is not important in the RH variance component. Thus, a constant variance component is used for RH.

To further capture the autocorrelation within each covariate and the correlation among different covariates, a VAR model with lag two [i.e., VAR(2)] is used. In particular, the error term is modeled by

$$\begin{bmatrix} \varepsilon_1(\tau) \\ \varepsilon_2(\tau) \\ \varepsilon_3(\tau) \end{bmatrix} = \Phi_1 \begin{bmatrix} \varepsilon_1(\tau-1) \\ \varepsilon_2(\tau-1) \\ \varepsilon_3(\tau-1) \end{bmatrix} + \Phi_2 \begin{bmatrix} \varepsilon_1(\tau-2) \\ \varepsilon_2(\tau-2) \\ \varepsilon_3(\tau-2) \end{bmatrix} + \begin{bmatrix} e_1(\tau) \\ e_2(\tau) \\ e_3(\tau) \end{bmatrix}, \quad (7)$$

where Φ_1 and Φ_2 are matrices of regression coefficients, and $[e_1(\tau), e_2(\tau), e_3(\tau)]' \sim N(0, \Sigma_e)$ are multivariate normal error terms that are independent over time. Here, Σ_e is the covariance matrix for the error terms. For the weathering example, the model fitting suggested that this VAR(2) model is adequate. For the weathering data, all covariate information was collected at the same place. When the units are exposed at different locations, additional parameters may be needed to describe the covariate processes.

6.3 Parameter Estimation

The estimation of the parameters in models (6) and (7) is done in two steps. In the first step, ML estimation is used to remove the seasonal trends in the mean and variance structures. Then the residuals are obtained. For the first stage, the working variance-covariance structure of $[\varepsilon_1(\tau), \varepsilon_2(\tau), \varepsilon_3(\tau)]'$ is taken to be $\sigma_\varepsilon^2 I_3$. The main goal of model (6) is to remove the mean structure and the simplified variance structure still provides a consistent estimator for the mean structure. The ML method is used to obtain the parameter estimates for the model in (6). One needs to program the likelihood function and then use an optimization algorithm (e.g., `optim()` function in R 2013) to maximize it. The convergence of the optimization algorithm is checked by trying different starting values and careful examination of the contour plots of the log-likelihood functions. The estimates of the parameters and corresponding bootstrap CIs for the covariate process model in (6) are listed in Table 2. We used a bias-corrected bootstrap approach with 10,000 repeats to obtain CIs. The bootstrap took about 20 min by using R parallel computing with 20 cores with Intel CPU (Xeon, E6540, 2.00GHz). Figure 1(b)–1(d) shows the fitted mean structure. Figure 8 shows the estimated error terms, and the estimated standard deviation (SD) of the error term for UV dosage, temperature, and RH. The figure shows that model (6) adequately fits the mean and variance structures (including the nonconstant variance pattern) for the UV dosage, temperature, and RH covariate process data.

In the second step, ML estimation is used to fit the VAR model to the residuals. The computing of the parameter estimates uses multivariate least squares (e.g., Lütkepohl 2005, chap. 3), which is computationally efficient. The estimates of Φ_1, Φ_2, and Σ_e are as follows:

$$\Phi_1 = \begin{pmatrix} 0.58 & 0.02 & 0.02 \\ 0.09 & 0.63 & 0.02 \\ -0.07 & -0.05 & 0.59 \end{pmatrix},$$

$$\Phi_2 = \begin{pmatrix} -0.11 & -0.02 & -0.01 \\ -0.11 & 0.03 & 0.02 \\ 0.39 & -0.11 & -0.11 \end{pmatrix},$$

Table 2. Parameter estimates and corresponding 95% bootstrap CIs for the parameters of the covariate process model in (6)

Covariate	Parameter	Estimate	Standard error	95% Bootstrap CI Lower	95% Bootstrap CI Upper
UV dosage	μ_1	24.71	0.58	23.55	25.83
	κ_1	18.95	0.71	17.54	20.32
	η_1	79.24	2.09	75.25	83.40
	ς_1	77.69	3.67	70.44	84.86
	ν_1	1.80	0.24	1.37	2.29
Temperature	μ_2	25.05	0.52	24.04	26.05
	κ_2	16.54	0.69	15.17	17.91
	η_2	103.19	2.65	97.92	108.27
	ς_1	33.53	13.73	6.96	60.66
	ν_2	0.31	0.09	0.14	0.49
RH	μ_3	40.01	1.02	38.06	42.06
	κ_3	–4.73	1.52	–7.38	–0.54
	η_3	39.00	18.8	6.71	80.23

$$\Sigma_e = \begin{pmatrix} 8.87 & 4.08 & -20.07 \\ 4.08 & 19.18 & -43.64 \\ -20.07 & -43.64 & 200.96 \end{pmatrix}. \quad (8)$$

The standard errors of the parameter estimates of Φ_1, Φ_2, and Σ are also obtained by using the bootstrap method. These standard errors are listed in supplementary Section 7. The bootstrap is carried out by sampling the estimated error term $[e_1(\tau), e_2(\tau), e_3(\tau)]'$ with replacement and then using the parametric models in (6) and (7) to obtain a bootstrap sample. The bootstrap values of the parameter estimates are obtained by using a two-step approach. The above process is repeated a large number of times to obtain the bootstrap distribution of parameter estimators.

We also examined the autocorrelation function (ACF) of the estimated $[e_1(\tau), e_2(\tau), e_3(\tau)]'$ to check the assumption of the VAR model (see supplementary Figure 8). The ACF functions showed no evidence of autocorrelation. We also used Q–Q plot to check the normal assumption on $[e_1(\tau), e_2(\tau), e_3(\tau)]$ (supplementary Figure 9). The plots show that the VAR(2) model with normal errors provides an adequate description of the residuals.

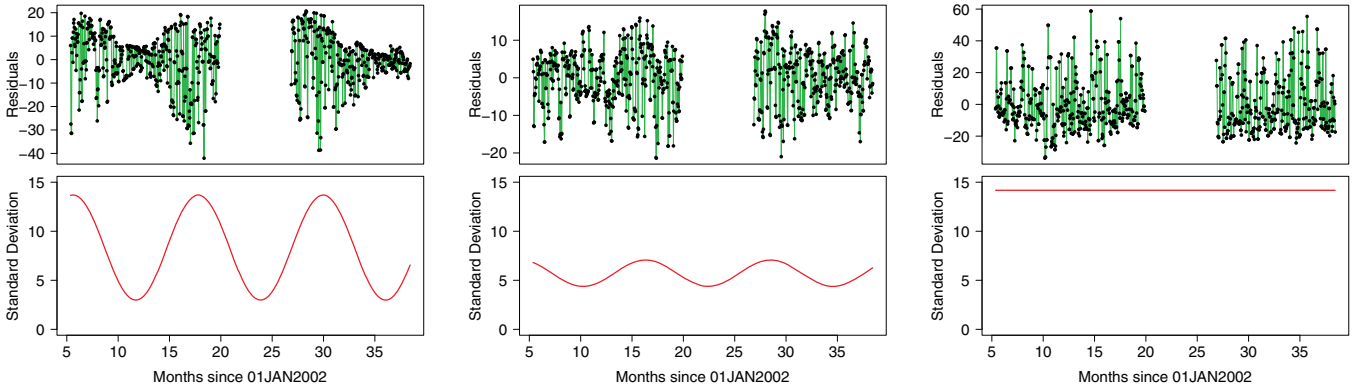

Figure 8. Residuals and estimated SD for UV dosage, temperature, and RH.

7. FAILURE-TIME DISTRIBUTION ESTIMATION

7.1 Failure-Time Distribution for the Population

The failure-time distribution provides the reliability information for an unobserved population. We use $\boldsymbol{\theta}_D$ and $\boldsymbol{\theta}_X$ to denote the unknown parameters in the degradation model and covariate process model, respectively. Let $\boldsymbol{\theta} = \{\boldsymbol{\theta}_D, \boldsymbol{\theta}_X\}$. The model for the actual path is $D[t; \boldsymbol{X}(\infty)] + R(t; w)$. Given the covariate process $\boldsymbol{X}(\infty) = \boldsymbol{x}(\infty)$ and the individual random effect w, the degradation path is deterministic. The first crossing (failure) time $t_{\mathcal{D}}$ for a particular unit can be obtained. That is,

$$t_{\mathcal{D}} = \min\{t : D[t; \boldsymbol{x}(\infty)] + R(t; w) = \mathcal{D}_f\}. \tag{9}$$

Thus, the first crossing time $t_{\mathcal{D}}$ is a function of $\mathcal{D}_f$, $\boldsymbol{x}(\infty)$, and w. Numerical methods are often needed to solve for t_D from (8). Because $\boldsymbol{X}(\infty)$ and w are random, the first crossing time (i.e., the failure time of the product), denoted by T, is a random variable. The cdf of $T = T[\mathcal{D}_f, \boldsymbol{X}(\infty), w]$ is

$$F(t; \boldsymbol{\theta}) = \mathbf{E}_{\boldsymbol{X}(\infty)} \mathbf{E}_w \Pr\left\{T[\mathcal{D}_f, \boldsymbol{X}(\infty), w] \le t\right\}, \quad t > 0. \tag{10}$$

In most situations, there is no explicit form for $F(t; \boldsymbol{\theta})$ and it has to be computed by using numerical methods or Monte Carlo simulation.

Substituting $\widehat{\boldsymbol{\theta}}$ into $F(t; \boldsymbol{\theta})$ in (9), one obtains an estimate of the cdf. Because an explicit form for $F(t; \widehat{\boldsymbol{\theta}})$ is, in general, not available, a simulation approach is used to evaluate $F(t; \widehat{\boldsymbol{\theta}})$. The following algorithm is used for computing $F(t; \widehat{\boldsymbol{\theta}})$.

Algorithm 2:

1. Simulate the covariate process with the parameter equal to $\widehat{\boldsymbol{\theta}}_X$.
2. Simulate the random effect w from $\mathrm{N}(0, \Sigma_w)$ with the parameter equal to $\widehat{\boldsymbol{\theta}}_D$.
3. Compute the simulated degradation path $D[t; \boldsymbol{X}(\infty)] + R(t; w)$ with the simulated covariate process and random effect.
4. Given the simulated degradation path, compute the failure time $t_{\mathcal{D}}$ by solving (8).
5. Repeat the above Steps 1 to 4 B times to obtain the simulated failure times $t^b_{\mathcal{D}}, b = 1, \ldots, B$, where B is chosen large enough to provide sufficient precision. The estimate of $F(t; \boldsymbol{\theta})$ is obtained by the empirical cdf. That is, $F(t; \widehat{\boldsymbol{\theta}}) = B^{-1} \sum_{b=1}^{B} \mathbb{1}_{(t^b_{\mathcal{D}} \le t)}$.

The CIs for the cdf can be obtained as follows. Because the bootstrap parameters $\widehat{\boldsymbol{\theta}}$ are obtained in previous sections, one needs to repeat Algorithm 2 for each set of bootstrap values of parameter estimates. The pointwise CIs for the cdf are then obtained as the sample quantiles of the bootstrap estimates of $F(t; \boldsymbol{\theta})$. If the focus is on an individual unit, Algorithm 2 can also be used to obtain the estimates for the cdf of an individual unit.

The manner in which our model and inference procedures would be used in applications will depend on relationship between the units of interest and the processes generating the covariates that will affect the degradation processes. Some example scenarios is as follows:

1. In some applications all units in the population will be subject to different realizations of a covariate processes that could be adequately modeled as independent (but not identically distributed) from unit to unit (location to location). For example, when considering the loss of light output from LED lights in households, the usage history is different but can be considered to be independent from household to household.
2. Similar to the groups of units in the weathering experiment, one might be interested in estimating the failure-time distribution of a population of units that are all subject to the same realization from the covariate processes. For example, when considering the power output decrease of solar panels installed at one location (e.g., one power plant), the environmental variables such as temperature and humidity can be considered to be the same for each unit in the field.
3. Similar to the overall weathering experiment, one might be interested in groups of units put into service at various points in time (known as staggered entry) so that the groups are subject to different parts of the same covariate process. The illustrative outdoor weathering example in this article falls into this category.

7.2 Application to the Epoxy Degradation Example

To illustrate the use of our methods, we use the outdoor weathering setting and assume that there is a hypothetical population with infinite size and that units randomly enter service, according to a uniform distribution, between day 161 and day 190. Each unit has its own independent realization of the covariate processes, from the observed processes in the experiment. Figure 9 shows the estimated cdf and the corresponding 95% pointwise CIs for this hypothetical population. For the results in Figure 9, we used $B = 200$ in Algorithm 2 with 10,000 bootstrap results already stored. The computations took about 1 hr by using R parallel computing with 20 cores with Intel CPU (Xeon, E6540, 2.00GHz). Most of the units in the population fail between 50 days and 150 days after they are put into service. Similar results can be obtained for the cdf of an individual unit (e.g., a unit started at day 161).

For the outdoor weathering data, we also checked how well the failure-time model fits the observed failure times. For the weathering data, we use a failure threshold $\mathcal{D}_f = -0.4$. Generally, this would be chosen to be the level of degradation at which the performance of the coating would not be acceptable (e.g., the level at which there would be customer perceivable loss of gloss or color). There were 36 units that were put into experiments at different times from 2002 to 2006 (i.e., in a staggered entry pattern). According to this failure definition, there were 17 failures and the other 19 units had survived.

Figure 10 shows the estimated expected number of failures and corresponding 95% pointwise CIs versus the observed number of failures as a function of time for the 36 specimens in the outdoor weathering data, conditional on the covariate history. The dots show the observed cumulative number of failures as a function of time. The estimated expected number of events are computed based on the estimated degradation path and covariate process models. For the periods from day 0 to day 597 and from day 806 to day 1153, the covariate processes for the weathering data had already been observed. We treat the covariates as fixed

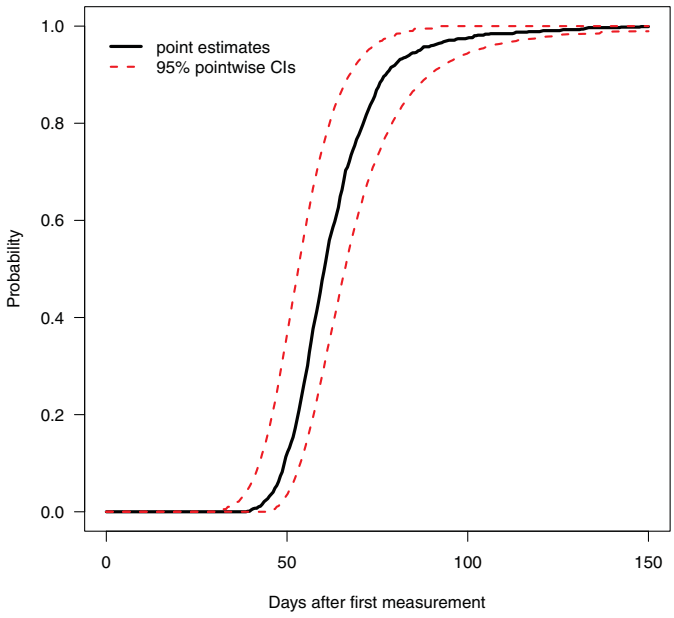

Figure 9. The estimated cdf and corresponding 95% pointwise CIs for a population with units starting randomly from day 161 to day 190.

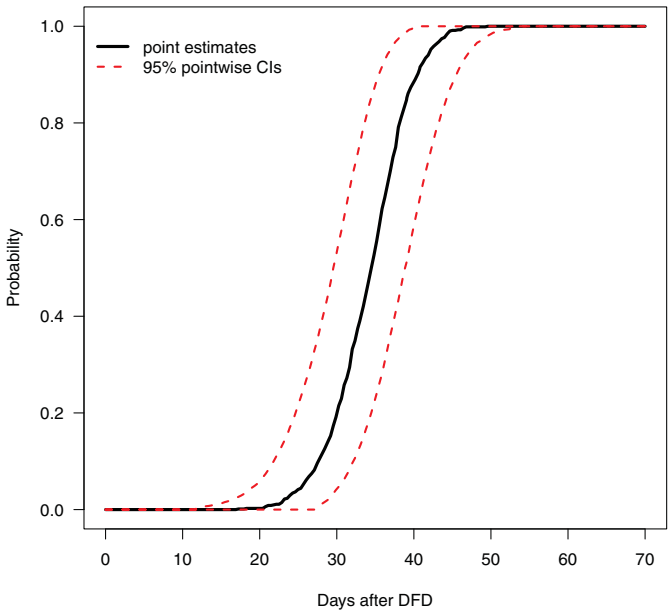

Figure 11. The estimated cdf of remaining life and 95% pointwise CIs for unit G18-10.

when we compute the estimated expected number of failures. For those periods that are between day 598 and day 805 and after day 1153, as shown in Figure 1, the covariate information is missing. The covariate process for those periods, however, is needed to compute the estimated expected number of events. We used multiple realizations of the covariate processes simulated from the fitted model and the results were averaged for those periods. The results in Figure 10 show that the estimated expected number of failures agree with the observed number of failures well except that there is an abrupt jump around day 50 in the observed number of failures.

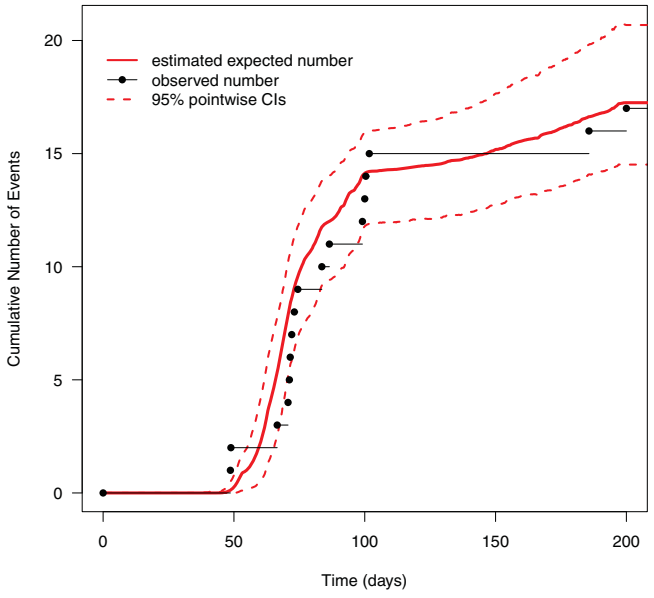

Figure 10. Estimated expected number of failures and corresponding 95% pointwise CIs versus the observed number of failures as a function of time for the 36 specimens in the outdoor weathering data, conditional on the covariate history.

7.3 Distribution of Remaining Life for Individual Units

Given the observed degradation path and the covariate process up to time t_{in_i} for individual i, the distribution of remaining life is needed in some applications. The conditional distribution of remaining life for individual with $\boldsymbol{X}_i(t_{in_i}) = \boldsymbol{x}_i(t_{in_i})$ and $T > t_{in_i}$ is

$$\rho_i(s;\boldsymbol{\theta}) = \mathbf{E}_{\boldsymbol{X}_i(\infty)|\boldsymbol{X}_i(t_{in_i})=\boldsymbol{x}_i(t_{in_i})}\mathbf{E}_w \Pr\big\{T[\mathcal{D}_f, \boldsymbol{X}(\infty), w] \le t_{in_i} + s | T > t_{in_i}\big\}, s > 0.$$

Here $\rho_i(s;\boldsymbol{\theta})$ gives, conditional on $\boldsymbol{X}_i(t_{in_i}) = \boldsymbol{x}_i(t_{in_i})$ and $T > t_{in_i}$, the probability of failure before time s. Similar algorithms can be used to evaluate the conditional distribution $\rho_i(s;\widehat{\boldsymbol{\theta}})$ for individual i and the corresponding pointwise CIs. The difference is that the future degradation path and the covariate process are conditional on $\boldsymbol{x}_i(t_{in_i})$ and the degradation measurements that have been observed up to time t_{in_i}.

For illustration, we consider the specimen labeled "G18-10" with age of 158 days at the end of exposure. The observed degradation level for G18-10 had not reached $\mathcal{D}_f = -0.4$ after 158 days. Conditional on the observed degradation path and the covariate history for this unit, we can compute the estimated cdf of remaining life for this unit. Figure 11 shows the estimated conditional cdf for unit G18-10 and the corresponding 95% pointwise CIs. The results in Figure 11 show that the remaining life of this unit is roughly in the range of 20 days to 50 days. The back test in supplementary Section 8 also shows that the remaining life can be predicted well by using the proposed method in this article.

8. CONCLUDING REMARKS AND AREAS FOR FUTURE RESEARCH

Motivated by the increasing availability of dynamic covariate information being acquired by systems operating in the field and the needs to predict future performance of these systems, we

develop a class of models and methods for using such data. We illustrate these methods with the outdoor weathering data. We use flexible general path models with individual random components to describe unit-to-unit variability in the data. Parametric models are used to model the covariate processes. We develop algorithms to compute an estimate for the failure-time distribution induced by the underlying degradation model. We use the weathering data to illustrate the modeling process and the estimation of the failure-time distribution.

Although the outdoor weathering data were our motivating example, the methods developed in this article can have broad applications for many products used in highly variable environments and/or subject to time-varying usages. For example, the degradation of LED power output is mainly due to usage that can be time varying. The corrosion of a crude oil transportation pipeline is subject to the outdoor environment and the characteristics of the compounds flowing in the pipeline. Damage done to structures in aircraft will depend on the number of takeoff–landing cycles and other stresses encountered during operation. Also, the degradation of photovoltaic arrays can be caused by both time-varying usage and outdoor environments. Thus, there are tremendous opportunities to apply the method developed.

For weathering applications, in the past decades, many solar UV monitoring sites have been established at different geographical locations within the United States and worldwide (e.g., Kaetzel 2001). The solar UV spectrum and intensity, as well as temperature and relative humidity are recorded at high resolution. Such information can be used for prediction for the lifetime of products that are subject to photodegradation. When the covariate information is from different locations, spatial correlations may need to be considered for the model to predict the covariates for a population. Spatial data modeling techniques can be applied. In other applications, where the product is not exposed to sunlight or other weather variables, our models can still be used to model degradation as a function of other variables like load or amount of use.

The covariate-effect function based on splines are only defined over the range of the data. As with all other nonparametric methods, extrapolation will be challenging. In the weathering data, there is enough historical data to cover the needed range of covariates. The shape-restricted spline, however, allows one to do extrapolation to some extent. Suppose, for example, that the possible range of a covariate is $[z_1, z_2]$ but the data only cover a range $[z_1 + \delta, z_2 - \delta]$ for a small positive δ. If the covariate-effect function is constrained to be monotone increasing, one can construct spline basis with z_1 and z_2 as boundary knots with other interior knots placed between $[z_1 + \delta, z_2 - \delta]$. Then estimate of the covariate-effect function can still be obtained over the range $[z_1, z_2]$. In this case, δ should be relatively small compared to the entire data range. Extrapolation based on monotone splines would be an interesting topic to investigate in future research.

The additive model for degradation paths proposed in this article is equivalent to a linear degradation path when the covariates are time invariant. In the future, it will be useful to consider a degradation path $\mathcal{D}(t) = g\{D[t; \boldsymbol{x}(t)] + R(t; w)\}$, where $g(\cdot)$ is a nonlinear function that depends on some unknown parameters. The estimation for such a model will, however, be challenging. We did not consider interactions between covariates in the model and it would be interesting to consider interaction effects in future research. It is, however, practically challenging to impose shape restriction so that the covariate-effect functions have physical meaning. Also, there needs to be enough data points to estimate the interaction effects.

There is a significant amount of research that has been done in the area of functional regression (e.g., Müller and Zhang 2005; Yao, Müller, and Wang 2005; Liu and Müller 2008). The research on the application of functional regression to degradation data includes Zhou et al. (2014), which does not consider time-varying explanatory variables. There has been little work to consider shape restrictions on covariate-effect functions in the degradation setting. We believe shape restrictions are useful when we already have physical knowledge/preliminary information on the shape of a covariate-effect function. It would be interesting to investigate the application of function linear regression methods to degradation data with time-varying covariates that also incorporate physical and engineering knowledge.

Regarding the parameter estimation for linear mixed-effects models, restricted ML (REML) estimates often used to reduce the bias. Although our simulation study shows that bias is not a big concern in our model, it would be interesting to investigate the use of REML under constraints. For the parameter estimation of the covariate process, we used a two-step approach. It would also be interesting to consider other approaches such as the expectation-maximization algorithm, by treating the $\varepsilon(\tau)$'s in (6) as missing data.

SUPPLEMENTARY MATERIALS

The following supplementary materials are available online.

Additional details: Additional algorithms, graphs and details on simulation results (pdf file).

Code and data: R code for Algorithms 1-4, simulations and data analysis. The NIST weathering data are also included (zip file).

ACKNOWLEDGMENTS

The authors thank the Editor, an associate editor, and the referees, for their valuable comments that helped in improving this article. The authors acknowledge Advanced Research Computing at Virginia Tech for providing computational resources. The work by Hong and Duan was supported by the National Science Foundation under Grant CMMI-1068933 to Virginia Tech and the 2011 DuPont Young Professor Grant.

[Received October 2012. Revised March 2014.]

REFERENCES

Bagdonavičius, V., Masiulaitytė, I., and Nikulin, M. S. (2010), "Reliability Estimation From Failure-Degradation Data With Covariates," in *Advances in Degradation Modeling: Applications to Reliability, Survival Analysis, and Finance*, eds. M. S. Nikulin, N. Limnios, N. Balakrishnan, W. Kahle, and C. Huber-Carol, Boston, MA: Birkhäuser. [181]

Bagdonavičius, V., and Nikulin, M. S. (2001a), *Accelerated Life Models: Modeling and Statistical Analysis*, Boca Raton, FL: Chapman & Hall/CRC. [181]

——— (2001b), "Estimation in Degradation Models With Explanatory Variables," *Lifetime Data Analysis*, 7, 85–103. [181]

Campbell, S. D., and Diebold, F. X. (2005), "Weather Forecasting for Weather Derivatives," *Journal of the American Statistical Association*, 100, 6–16. [188]

Carpenter, J. R., Goldstein, H., and Rasbash, J. (2003), "A Novel Bootstrap Procedure for Assessing the Relationship Between Class Size and Achievement," *Applied Statistics*, 52, 431–443. [185]

Davidov, O., and Rosen, S. (2011), "Constrained Inference in Mixed-Effects Models for Longitudinal Data With Application to Hearing Loss," *Biostatistics*, 12, 327–340. [184]

Efron, B., and Tibshirani, R. (1993), *An Introduction to the Bootstrap*, Boca Raton, FL: Chapman and Hall/CRC. [185]

Eilers, P. H. C., and Marx, B. D. (1996), "Flexible Smoothing With B-Splines and Penalties," *Statistical Science*, 11, 89–121. [185]

Escobar, L. A., Meeker, W. Q., Kugler, D. L., and Kramer, L. L. (2003), "Accelerated Destructive Degradation Tests: Data, Models, and Analysis," in *Mathematical and Statistical Methods in Reliability*, eds. B. H. Lindqvist and K. A. Doksum, Singapore: World Scientific Publishing Company. [181]

Fraser, D. A. S., and Massam, H. (1989), "A Mixed Primal-Dual Bases Algorithm for Regression Under Inequality Constraints. Application to Concave Regression," *Scandinavian Journal of Statistics*, 16, 65–74. [184]

Gu, X., Dickens, B., Stanley, D., Byrd, W. E., Nguyen, T., Vaca-Trigo, I., Meeker, W. Q., Chin, J. W., and Martin, J. W. (2009), "Linking Accelerating Laboratory Test With Outdoor Performance Results for a Model Epoxy Coating System," in *Service Life Prediction of Polymeric Materials*, eds. J. Martin, R. A. Ryntz, J. Chin, and R. A. Dickie, New York: Springer. [181,184]

Joseph, V. R., and Yu, I. (2006), "Reliability Improvement Experiments With Degradation Data," *IEEE Transactions on Reliability*, 55, 149–157. [181]

Kaetzel, L. J. (2001), "Data Management and a Spectral Solar UV Network," in *Service Life Prediction Methodologies and Metrologies, American Chemical Society Symposium Series* (Vol. 805), eds. J. W. Martin and D. R. Bauer, New York: Oxford Press. [192]

Lawless, J. F., and Crowder, M. (2004), "Covariates and Random Effects in a Gamma Process Model With Application to Degradation and Failure," *Lifetime Data Analysis*, 10, 213–227. [181]

Liu, B., and Müller, H.-G. (2008), "Functional Data Analysis for Sparse Auction Data," in *Statistical Methods in e-Commerce Research*, eds. W. Jank and G. Shmueli, Hoboken: Wiley. [192]

Liu, Q., and Pierce, D. A. (1994), "A Note on Gauss-Hermite Quadrature," *Biometrika*, 81, 624–629. [184]

Lu, C. J., and Meeker, W. Q. (1993), "Using Degradation Measures to Estimate a Time-to-Failure Distribution," *Technometrics*, 34, 161–174. [181]

Lütkepohl, H. (2005), *New Introduction to Multiple Time Series Analysis* (2nd ed.), Berlin: Springer-Verlag. [189]

Meeker, W. Q., and Escobar, L. A. (1998), *Statistical Methods for Reliability Data*, New York: Wiley. [183]

Meeker, W. Q., Escobar, L. A., and Lu, C. J. (1998), "Accelerated Degradation Tests: Modeling and Analysis," *Technometrics*, 40, 89–99. [181]

Meyer, M. C. (2008), "Inference Using Shape-Restricted Regression Splines," *The Annals of Applied Statistics*, 2, 1013–1033. [183,185]

Morris, J. S. (2002), "The BLUPs Are Not 'Best' When It Comes to Bootstrapping," *Statistics and Probability Letters*, 56, 425–430. [185]

Müller, H.-G., and Zhang, Y. (2005), "Time-Varying Functional Regression for Predicting Remaining Lifetime Distributions From Longitudinal Trajectories," *Biometrics*, 61, 1064–1075. [192]

Nelson, W. (2001), "Prediction of Field Reliability of Units, Each Under Differing Dynamic Stresses, From Accelerated Test Data," in *Handbook of Statistics 20: Advances in Reliability*, eds. N. Balakrishnan and C. R. Rao, Amsterdam: North-Holland. [181,183]

Park, C., and Padgett, W. J. (2006), "Stochastic Degradation Models With Several Accelerating Variables," *IEEE Transactions on Reliability*, 55, 379–390. [181]

R Development Core Team (2013), *R: A Language and Environment for Statistical Computing*, Vienna, Austria: R Foundation for Statistical Computing. [189]

Reinsel, G. C. (2003), *Elements of Multivariate Time Series Analysis* (2nd ed.), New York: Springer-Verlag. [188]

Self, S. G., and Liang, K.-Y. (1987), "Asymptotic Properties of Maximum Likelihood Estimators and Likelihood Ratio Tests Under Nonstandard Conditions," *Journal of the American Statistical Association*, 82, 605–610. [185]

Singpurwalla, N. D. (1995), "Survival in Dynamic Environments," *Statistical Science*, 10, 86–103. [181]

Yao, F., Müller, H.-G., and Wang, J.-L. (2005), "Functional Linear Regression Analysis for Longitudinal Data," *The Annals of Statistics*, 33, 2873–2903. [192]

Zhou, R., Serban, N., Gebraeel, N., and Müller, H.-G. (2014), "A Functional Time Warping Approach to Modeling and Monitoring Truncated Degradation Signals," *Technometrics*, 56, 67–77. [181,192]